Sodium Percarbonate Based Mixed Media Fuel Cells Supported on Paper with Au/NiO Catalysts

Rajat Verma,[*] Sweta Lal,[†] Melepurath Deepa,[‡§] Vinod M. Janardhanan, [¶]
Kirti Chandra Sahu[‖]

Abstract

Self-pumping T-shaped mixed media paper based fuel cells are implemented using sodium percarbonate as a fuel, $KMnO_4$ as an oxidant and a proton conducting gel as the electrolyte for the first time. Whatman filter papers serve as porous supports for the fluid (catholyte and anolyte) streams. The cell architecture with Au/NiO (with 11 wt% Au) composite as the catalyst deposited at both electrodes, delivers the highest current and power densities of 5.6 mA cm^{-2} and 2.6 mW cm^{-2}, respectively. With catalyst, the maximum current and power densities are enhanced by 75% and 121%, respectively. Impedance analysis showed that Ohmic and polarization resistances reduce significantly by use of the Au/NiO (with 11 wt% Au) composite as catalyst. The ability of this cell to revive and restore its original performance once both open circuit voltage and current density have decayed, clearly demonstrates the applicability of this robust, easily disposable cell for powering micro-nano devices.

1 Introduction

Laminar flow membraneless fuel cells have received significant attention in the recent past as ideal candidates for power generation in the milliwatts range [1, 2, 3, 4]. These devices differ from the conventional fuel cells that use a physical membrane to keep the fuel and oxidant streams separated. In laminar flow based membraneless fuel cells, the fuel and the oxidant streams come in contact with each other, but the mixing is confined to the liquid-liquid interface formed between the two parallel flowing streams [5, 6, 7]. This interface acts as a virtual membrane, which allows the transport of ions from one electrode to the other. Due to the absence of a membrane, the electrolyte transport in these cells is achieved by mixing the fuel and oxidant with appropriate electrolytes, thus forming the anolyte and catholyte. These cells consume reagents in very small quantities and therefore the power produced by these cells is also proportionally low. The absence of membrane eliminates several complexities associated with electrolyte membrane development and its optimization. However, the requirement of a metering mechanism for anolyte and catholyte limits the use of membraneless cells in micro electronics and sensing devices.

Recently, there have been reports on the use of paper as a transport medium for the anolyte and catholyte [8, 9, 10, 15]. The principle behind the working of these fuel cells is similar to that of laminar flow membraneless fuel cells. However, the mixing of anolyte and catholyte in these cells are spread over a much wider region near the liquid-liquid interface and therefore the life of these cells is shorter compared to laminar flow cells. However, paper based cells do have the advantage that external devices are not required for the metering of the anolyte and the catholyte. The anolyte

[*]R. Verma, Department of Chemistry, Indian Institute of Technology Hyderabad, Kandi, 502 285, Sangareddy, Telangana, India
[†]S. Lal, Department of Chemical Engineering, Indian Institute of Technology Hyderabad, Kandi, 502 285, Sangareddy, Telangana, India
[‡]Corresponding authors:vj@iith.ac.in and mdeepa@iith.ac.in
[§]Dr. M. Deepa, Department of Chemistry, Indian Institute of Technology Hyderabad, Kandi, 502 285, Sangareddy, Telangana, India
[¶]Dr. V. M. Janardhanan, Department of Chemical Engineering, Indian Institute of Technology Hyderabad, Kandi, 502 285, Sangareddy, Telangana, India
[‖]Dr. K. C. Sahu, Department of Chemical Engineering, Indian Institute of Technology Hyderabad, Kandi, 502 285, Sangareddy, Telangana, India

and the catholyte are transported to the respective electrodes due to the intrinsic physical properties of paper. Similar to laminar flow membraneless fuel cells, paper based cells also deliver power in the range of milli-watts. Paper based cells also have advantages of ease of construction, ease of disposal after use, fuel flexibility and portability.

Electrochemical performance of membraneless fuel cells and hence paper based fuel cells depends largely on the redox couple chosen. Since these cells deliver only a few milli amperes of current, a high standard cell potential is often preferred to obtain a reasonable power density. The standard cell potential depends on the reduction potential of the fuel and the oxidant. Since the fuel and the oxidant are mixed with the electrolyte for the former to be ionically conductive, the chemistry of these cells is much more complex than that of a conventional fuel cell. Many a times, the ions that migrate to the opposite electrode need not be released from the fuel or oxidant, rather in these cells, the ions may be liberated from the electrolyte. For instance in the hydrazine (N_2H_4)/hydrogen peroxide (H_2O_2) cell reported by Yan et al. [11], NaOH and H_2SO_4 are used as electrolyte phases along with the fuel and the oxidant respectively. Here, the OH^- ions liberated from NaOH reacts with N_2H_4 at the anode and the H^+ ions liberated from H_2SO_4 reacts with H_2O_2 at the cathode. It should be noticed that a base is used as an electrolyte phase on the fuel side and an acid is used as an electrolyte phase on the oxidant side forming a mixed media cell.

Among various liquid fuels, which can be handled and streamed at ambient temperature such as formic acid, methanol, hydrazine and so forth [12], sodium percarbonate (SPC, $Na_2CO_3.1.5H_2O_2$) is remarkable due to many reasons. It is an adduct of sodium carbonate and hydrogen peroxide [13, 14], and in aqueous medium, it releases H_2O_2 that undergoes oxidation at the anode. It is non-toxic, biodegradable and environmentally safe [13]. It is non-flammable, non-explosive, inexpensive and easy to handle. It also does not produce harmful by-products after oxidation in an alkaline medium [4]. These characteristics render SPC to be a versatile fuel. Similarly, an aqueous acidic solution of potassium permanganate also serves as a powerful oxidant at room temperature, and can be directly fed to the paper strip as a catholyte stream, during cell operation [16]. The combination of SPC as the fuel, and $KMnO_4$ as the oxidant, also yields a high theoretical open circuit voltage (OCV) of 1.57 V, and therefore this fuel-oxidant combination is employed in this study.

While there are a plethora of metallic and non-metallic catalysts those have been employed in low cost- microbial and paper based fuel cells, such as platinum and gold [8, 17, 18], here we used gold nanoparticles (Au NPs) and nickel oxide (NiO) microspheres, and their composite (Au/NiO) as catalysts and studied the effect of these catalysts on the electrochemical response of paper based fuel cells. Previously, a bimetallic alloy at an optimum composition of $Au_{85}Ni_{15}$ and prepared by a phase separation mechanism, showed high electrocatalytic activity for formic acid oxidation [19]. The same catalyst and Au@Ni core shell nanoparticles also showed good activity for oxygen reduction in a low temperature solid oxide fuel cell [20, 21], thus indicating that Au/NiO composite catalysts as prepared herein, are suitable for application to cells which can deliver high power densities. These materials offer high electronic conductivities and large effective surface areas, and thus satisfy the pre-requisites for application as catalysts in paper based fuel cells. Among current collectors, such as molybdenum, graphite, copper and platinum [22], graphite sheets are chosen for paper based fuel cells due to low cost, lightweight, high porosity (which can enable high catalyst loading), and chemical inertness [23].

Keeping in view the aforesaid aspects, in this work, we present the working and characterization of sodium percarbonate ($Na_2CO_3{\cdot}1.5H_2O_2$)/$KMnO_4$ fuel cells. Here, we have used SPC as the fuel and $KMnO_4$ as the oxidant. NaOH is used as the electrolyte on the anode side and H_2SO_4 is used as the electrolyte on the cathode side. Graphite sheet is used both as the electrode and current collector. Although paper based fuel cells reported so far, work on the principle of a membraneless fuel cell, here we use a proton conducting polymeric gel as the electrolyte between the two strips to complete the transfer of ions from one electrode to the other and to limit the mixing of the anolyte and catholyte streams at the same time. This cell assembly works as a self-pumping system, where fluids are kept in reservoirs, and the cell is supported on a glass substrate. Thus, the fabrication of this fuel cell assembly is facile and it is also exceedingly easy to regenerate the cell in very less time. Further, these cells can also be stacked in series or in parallel to fulfill the power required for operating higher current / voltage electrical devices, which could be used for more than half an hour and can be disposed easily.

2 Results and Discussion

Sodium percarbonate ($Na_2CO_3{\cdot}1.5H_2O_2$) releases H_2O_2 when dissolved in ultra pure water according to

$$2Na_2CO_3.3H_2O_2 \rightarrow 2Na_2CO_3 + 3H_2O_2. \tag{1}$$

The OH^- ions which are released from NaOH react with H_2O_2 according to

$$H_2O_2 + 2OH^- \rightarrow O_2 + 2H_2O + 2e^-, \quad E^0 = 0.0649\ V. \tag{2}$$

$KMnO_4$ is used as the oxidant whose concentration is kept throughout this study at 0.5 M. The catholyte is formed by adding 2 M H_2SO_4 to $KMnO_4$. The reaction at the cathode proceeds according to

$$MnO_4^- + 8H^+ + 5e^- \rightarrow Mn^{2+} + 4H_2O, \quad E^0 = 1.546\ V. \tag{3}$$

The overall cell reaction follows

$$2MnO_4^- + 6H^+ + +5H_2O_2 \rightarrow 2Mn^{2+} + 8H_2O + 5O_2 \tag{4}$$

with a standard cell potential of 1.57 V. The cell assembly and fabrication are explained in the experimental section, and a schematic diagram illustrating the cell construction and a photograph of the cell are presented in Fig. 1(a) and (b), respectively. The variation of open circuit voltage (OCV) as a function of time is studied for different concentrations of the SPC. 2 M H_2SO_4 conducting gel is used to connect the two paper strips and the results are shown in Fig. 2. Every time a new cell is used to study a new concentration of SPC. To analyze the voltage drop, each cell is operated for 10 min. by using chronopotentiometry. At 6 M fuel concentration, the OCV is 1.31 V, and the drop from the initial value is less compared to the other concentrations studied. The OCV drops only by 0.03 V over a span of 10 min. for 6 M. At time $t = 0$ s, the OCV for all concentrations are more or less the same. However, as time progresses, difference in behavior is observed. A drop in cell potential over time can occur either due to the accumulation of reaction products at the electrochemically active sites or due to fuel and oxidant cross over. Although the presence of gel electrolyte is expected to result in much more stable operation of the cell compared to a laminar flow paper based fuel cell, the difference in OCV for different fuel concentrations leads us to the inference that the gel does allow the transport of anolyte and/or catholyte to the other electrode. Although the cell maintained at 6 M provides better OCV as compared to the cell with 3 M, the former resulted in a turbid solution. Since a turbid solution results when the salt concentration present is in excess to that of saturation concentration, its difficult to determine the actual concentration of the resulting solution. Therefore, for the rest of the experiments we have used 3 M SPC, which is a clear solution.

The effect of SPC concentration on the cell performance is shown in Fig. 3. The concentration of SPC is varied from 0.5 M to 3 M. As the fuel concentration increases, the limiting current also increases with 3 M SPC resulting in a limiting current of 3.2 mA cm^{-2} and a maximum power density of 1.2 mW cm^{-2}. It is obvious from Fig. 3 that an increase in fuel concentration results in progressive improvement in cell performance. However, the same is not true in the case of cell stability study at OCV (Fig. 2). An increase in cell performance with increase in fuel concentration is an expected behavior. Since the current densities produced by these cells are very low, the fuel consumption will also be proportionally low and a very large concentration of fuel at the anode would render the exchange current density a sole function of fuel concentration as the dilution effect due to the product formation will be suppressed by the high fuel concentration. However, if the gel allows the fuel and oxidant to cross over, a higher fuel concentration can result in a lower cell performance. This effect has been reported in the case of paper based laminar flow cells [9]. Nevertheless, here we have not observed this reverse effect until 3 M SPC.

The effect of acid concentration in the gel on the cell performance is shown in Fig. 4. 1 M and 5 M acid concentrations in the gel lead to similar performances and the medium concentrations (2 M - 4 M) lead to slightly better performances compared to 1 M and 5 M concentrations. Considering the experimental errors, one can conclude that the acid concentration in the gel does not have much influence on the cell performance. For the rest of the results presented in the work, we have used 2 M acid concentration in the gel.

X-ray fluorescence (XRF) analyses of the anode and cathode strips are conducted to identify the elements that can migrate from one electrode to the other as a result of electrochemical reactions (see Table 1). At the anode, the XRF data reveals the presence of some amount of sulfur indicating the transport of SO_4^{2-} ions to the anode, which originates

from the cathode or from the gel. The XRF data of the cathode revealed only the presence of K, Mn, O and S. The gel electrolyte is composed of poly (acrylamide) and acid (H_2SO_4), and it is capable of conducting both Na^+ and SO_4^{2-} ions. During cell operation, Na^+ ions, which are released by sodium percarbonate decomposition in water at the anode, can move from the anode to the cathode via the electrolyte, and form Na_2SO_4 at the cathode, by combining with the SO_4^{2-} ions which are released by the acid (H_2SO_4) at the cathode upon reduction of permanganate ions. Alternatively, SO_4^{2-} ions can also migrate from the cathode to the anode, and combine with Na^+ ions to form Na_2SO_4 at the anode. From XRF, since we obtained evidence for the existence of sulfur at the anode, the second process is confirmed, for the fuel containing solution does not contain any sulfur based species. In a similar vein, the feasibility of the first process can also not be ruled out, thus indicating that both Na^+ and SO_4^{2-} ions can move across the gel in the above described directions during cell operation.

To enhance the electrochemical performance of the fuel cell, three catalysts are used: Au NPs, NiO and an Au/NiO (with 11 wt% Au) composite. The SEM images of Au NPs (Fig. 5(a) and 5(b)), show aggregated NPs, which are interconnected. The morphology of pristine NiO is composed of micro-spherical particles which have a flaky structure. The flaky texture implies a high catalytic area, which will be available for the electrochemical reactions (Fig. 5(c) and 5(d)). The morphology of the Au/NiO composite reveals the presence of inter-linked flaky quasi-spherical particles of NiO mixed with the irregular shaped Au NPs. The mixing appears to be moderately uniform and it is somewhat difficult to distinguish the Au NPs from the NiO particles in the composite (Fig. 5(e) and 5(f)).

Table 1: X-ray flouroescence (XRF) data of paper strips extracted from a T-shaped mixed media paper based fuel cell with 3 M SPC dissolved in 3 M NaOH as the fuel, 0.5 M $KMnO_4$ (in 2 M H_2SO_4) as the oxidant and a 2 M H^+ conducting gel as the electrolyte. Data: (a) for a strip from the fuel (anodic) side, and (b) for a strip from the oxidant (cathodic) side.

(a)
Fuel strip

Compound	Si	P	S	Cl	Ca	Mn	Fe
Concentration	3.98 %	5.585 %	58.58 %	17.497 %	12.951 %	0.825 %	0.584 %

Sample paper

Compound	Mg	Si	P	Cl	Ca	Fe
Concentration	21.462 %	10.35 %	15.049 %	24.225 %	27.93 %	0.984 %

(b)
Oxidant strip

Compound	Al	Si	P	S	Cl	K	Ca	Mn
Concentration	2.242 %	0.98 %	1.095 %	25.877 %	2.557 %	16.626 %	1.992 %	48.729 %

Sample paper

Compound	Mg	Si	P	Cl	Ca	Fe
Concentration	21.462 %	10.35 %	15.049 %	24.225 %	27.93 %	0.984 %

The TEM images of Au NPs, NiO and an Au/NiO (with 11 wt% Au) composite are shown in Fig. 6. The TEM images of Au NPs (Fig. 6(a)-Fig. 6(c)), show that the NPs are quasi-spherical, and their diameters lie in the range of 3 to 12 nm. The NPs are discrete in solution phase, and remain so due to the citrate ions (or capping agent) that ensconce the Au core, and thus prevent them from aggregation. Upon injection of the Au precursor containing the reducing agent (citrate), Ag^+ and $AuCl_4^-$ species at high temperature, a burst nucleation event occurs, which consumes most of the precursors, leading to fast nucleation and growth processes, and resulting in the formation of moderately small sized Au NPs, as obtained here. The role of Ag^+ ions here is to catalyze the oxidation of citrate, which in turn accelerates the conversion of $AuCl_4^-$ ions to Au^0-NPs.

The largest diameter achieved for an Au-NP here is 12 nm, and one such NP is displayed in Fig. 6(c). Au NPs are polycrystalline, and this is confirmed from the ring pattern superimposed with bright spots observed in the selected area electron diffraction (SAED) pattern of Au NPs (Fig. 6d). The spots on the rings are indexed to the (111), (220),

(311), (222) and (422) planes, corresponding to the inter-planar spacings (d) of 2.32, 1.43, 1.24, 1.15, and 0.83 Å, which match reasonably well with the d-values of the face centered cubic (fcc) lattice of Au, in concurrence with PDF (powder diffraction file) # 652870. Pristine NiO shows a flaky, floral morphology (Fig. 6(e) and (f)), wherein the floral shapes are again, almost spherical, which aligns with the SEM observations. The microspheres are composed of nano-sized flakes/sheets, and it is this texture which imparts a high catalytic surface area to pristine NiO. The floral-spherical shapes have diameters varying from 0.5 to 2.5 μm. The sheet/flake-like structure of the NiO micro-spheres is evident from Fig. 6(g). The SAED pattern of pristine NiO reveals concentric rings (Fig. 6(h)), and the rings are assigned to (111), (200), (220), (400) and (331) planes corresponding to inter-planar distances of 2.4, 1.95, 1.4, 1.01 and 0.8 Åof the fcc crystal structure of NiO, as per PDF # 47-1049. During the hydrothermal preparation of NiO and the Au/NiO composite, urea first decomposes to yield NH_3 and CO_2, and NH_3 and water combine to produce NH_4^+ and OH^- ions. The OH^- ions react with Ni^{2+} ions and $Ni(OH)_2$ is obtained, which further undergoes thermal oxidation to yield NiO. In this reaction phase, (i) the surfactant sodium dioctyl-sulfosuccinate (AOT) via templating effects- and (ii) the CO_2 bubbles produced in-situ, which serve as nucleating sites for NiO growth-, orchestrate the formation of the NiO micro-spherical floral shapes. During the course of preparation of the Au/NiO composites, the medium, namely, ethanol functions as a reductant, and reduces $AuCl_4^-$ to Au^0, and the ensuing Au^0 species tend to aggregate (in the absence of a capping agent). However the aggregation is contained to some extent by the presence of floral NiO structures, in the same reaction mixture. The Au NPs thus get embedded in the NiO micro-spheres, and the Au/NiO composites are obtained. The TEM image of the Au/NiO (with 11 wt% Au) composite shows that the NiO micro-spherical floral shapes are retained in the composite, and the dark contrast of the floral shapes indicates that Au NPs are implanted in the NiO-floral shapes (Fig. 6(i)). This is also confirmed from an enlarged view of the composite presented in Fig. 6(j). The image shows the presence of Au-NP aggregates, which too have spherical shapes to be embedded in the sheet/flake-like structures that constitute the NiO microspheres. The Au NPs show a wide variation in size, as the diameters vary from 3 to 75 nm. This broad size distribution is due to aggregation of Au NPs. Two SAED patterns extracted from this composite, are shown in Fig. 6(k) and (l), and these ring patterns match with the crystal structures of NiO and Au respectively. The ring patterns are indexed to the (111), (200), (220) and (400) planes of NiO (Fig. 6 (k)), and to the (111), (200), (220), (311), and (222) planes of Au (Fig. 6(l)); both with fcc lattices.

The UV-visible spectrum of Au NPs colloid, displayed in Fig. 7 shows a surface plasmon resonance peak at 519 nm, clearly indicating the formation of NPs. A photograph of the wine-red colored Au NPs is shown as an inset of Fig. 7(a). The XRD pattern for NiO particles is shown in Fig. 7(b), where the peaks expected from crystalline NiO with a face centered cubic structure are represented using asterisks and a photograph of the black colored NiO product is shown as an inset of Fig. 7(b). The XRD peaks of Au in the Au/NiO composite match with the diffraction peaks of Au with a face centered cubic lattice, with peaks observed at 2θ = 38.2, 44.2 and 64.05°, corresponding to d values of 2.35, 2.04 and 1.45 Å, which match with the (111), (200), and (220) planes (PDF: 652870). The positions where NiO peaks are expected, are marked with asterisks (Fig. 7(c)), but NiO obtained here is found to be amorphous. A black colored Au/NiO composite is shown as an inset of Fig. 7(c).

The performances of the cells with various catalysts at the anode and cathode are shown in Fig. 8. 3 M SPC in 3 M NaOH and 0.5 M $KMnO_4$ in 2 M H_2SO_4 are used as anolyte and catholyte respectively. Three different catalysts, namely Au NPs, NiO and composite of Au/NiO are used for evaluating the cell performance. Fig. 8(a) shows the performance of the cell with Au NPs as catalyst. The Au NPs are drop casted on the graphite electrode(s) and air-blow dried. The drop-casting is done thrice, and after each time, the electrodes are dried. The cell gave the best performance when Au NPs are used alone at the cathode. The effect of Au NPs when loaded at both electrodes leads to a similar cell performance. This is probably because of the relatively better stability of Au NPs in acidic environment at the cathode compared to the alkaline environment at the anode.

The NiO catalyst is dispersed in ethanol and then drop-casted on graphite electrode(s). Similar to Au NPs, NiO also gave better performance when used at the cathode alone relative to its use at the anode alone (Fig. 8(b)). The cell performance with NiO at both electrodes is similar to that of its use only at the cathode. The cell performance for the composite is shown in Fig. 8(c). The cell gave the best performance when the composite is used at both electrodes. Au/NiO composite (11 wt% Au) is dispersed in ethanol and this solution is used to drop cast the catalyst on the graphite electrodes. After drop casting the electrode is air blow dried. The cell produced a peak power density of 2.66 mW/cm^2. The performance of the composite when used only at the cathode is very much similar to the performance of the cell with NiO used only at the cathode (Fig. 8(b)). Moreover the performance of the composite is not dramatically different from the performance of Au NPs. In fact, on comparing the *IV* characteristic curves, the area specific resistance (ASR)

in the case of the composite is lower than that of Au NPs, which leads to better power density. However, the limiting currents are in similar range. The cell performance is also evaluated for other concentrations of Au (i.e., 5.11 wt% and 16.8 wt%). However, the performance is inferior compared to 11 wt% Au loading. The plots are shown in Fig. 9.

For studying the cell performance with various catalyst combinations, 3M SPC in 3M NaOH is used as the anolyte and 0.5M $KMnO_4$ in 2M H_2SO_4 is used as the catholyte. In this combination, the cathode is under an acidic environment and the anode is in an alkaline medium. The power density (cell performance) will differ depending on the catalysts ability to promote the oxidation and reduction reactions. Any increase in the rate of these reactions results in an increased exchange current density. The Au nanoparticles are capable of promoting both oxidation and reduction reactions and therefore, power density obtained with the use of Au nanoparticles is significantly higher compared to the power density obtained with plain graphite sheets. Similar increment in power density is obtained with the use of NiO on the cathode side. Since the use NiO at the anode led to a power density comparable only to that of plain graphite sheet, we can conclude that NiO catalyses only the reduction reaction. However, their synergetic effect leads to better cell power density when they are used at both anode and cathode. This is because the Au nanoparticles promote both oxidation and reduction reactions and NiO promotes the reduction reaction.

The sustainability of the cell at OCV for different catalysts used is shown in Fig. 10(a). In general, cells with catalysts lead to better stability compared to graphite sheet electrodes. With the composite electrode, the drop in voltage is only 0.08 V over a period of 30 min. Fig. 10(b) and 10(c) shows the performance of the cell with composite catalyst under part load conditions. At 2.1 mA, the cell produced a voltage of 0.8 V, however, dropped to 0 V in 10 min. This drop in voltage is due to the fuel and oxidant consumption and upon replenishing the cell with fresh fuel and oxidant, the cell voltage recovered back to its original value and again dropped to 0 V in another 10 min. When the cell is operated at 0.71 V, it produced a current of 5 mA and dropped to 1 mA in 20 min. Similar operation in galvanostatic mode showed that upon replenishing the fuel and oxidant, the cell is able to recover the current produced. Both Fig. 10(b) and (c) show that this cell has the ability to produce relatively stable current and voltage on continuous supply of fuel and oxidant.

The electrochemical impedance spectra of the cells without any catalyst for different fuel concentrations at OCV are shown in Fig. 11. The plots are recorded by applying a sinusoidal voltage perturbation of 10 mV in the frequency range of 1MHz to 0.1 Hz. Fig. 11(a) shows that the Ohmic resistance offered by the cell is unaffected by the fuel concentration. However, the polarization resistance of the cell decreased with increasing fuel concentration. Only a single arc is observed in all cases, probably because the charge transfer resistance of the oxidation reactions are insignificant compared to that of reduction. At low frequency, all fuel concentrations indicate the presence of mass transfer limitation. The depressed nature of semicircles in all cases also indicates that the capacitance contribution is not ideal. The Nyquist plot for the cell without catalyst at part load conditions is shown in Fig. 11(b). The polarization resistance offered by the cell under part load conditions is lower compared its operation at OCV. Similarly the Nyquist plots for the cell with catalyst at 3 M fuel concentration at OCV is shown in Fig. 11(c) and at part load condition of 0.71 V is shown in Fig. 11(d). In general the polarization resistance decreases with increasing current or decreasing cell voltage [27, 28]. The cell behavior agrees with this general trend for electrodes with and without catalyst.

3 Conclusions

Self-pumping T-shaped paper based fuel cells are assembled by using sodium percarbonate as a fuel and potassium permanganate as an oxidant with a proton conducting gel. This cell is light-weight and consumes very less fuel. It is portable and easily accessible. Whatman filter papers are used as porous supports for the fluids. The capillary action of the fluid on the porous paper allows the parallel streams of anolyte and catholyte. Mixed media and an acidic gel-electrolyte based cell gives a high OCV of 1.22 V at 3 M SPC fuel and 0.5 M $KMnO_4$ concentrations. The T-shaped mixed media paper based fuel cell produces a maximum current density of 3.21 mA/cm^2 and a maximum power density of 1.2 mW/cm^2 without any catalyst. The Au/NiO composite (with 11 wt% Au) as catalyst is found to be the best as the T-shaped mixed media paper based fuel cell with this catalyst delivered current and power densities of 5.6 mA/cm^2 and 2.66 mW/cm^2 respectively. This cell outperformed all other cell configurations, and is also found to be capable of regenerating its origional current and voltage produced after decay, by replenishment with fresh fuel/oxidant. Our study demonstrates that this low cost cell is an economically viable and an ecologically benign alternate to batteries for powering micro-nano devices.

4 Experimental Section

Chemicals

Sodium percarbonate ($Na_2CO_3.1.5H_2O_2$, H_2O_2: 20-30 %), acrylamide (C_3H_5NO, 99%), dioctyl sodium sulfosuccinate salt ($C_{20}H_{37}NaO_7S$, 96%), gold (III) chloride trihydrate ($HAuCl_4.3H_2O$, 99.9%), nickel nitrate ($Ni(NO_3)_2.6H_2O$, 99.99%), ammonium persulfate ($(NH_4)_2S_2O_8$, 98%), tri-sodium citrate dihydrate ($HOC(COONa)(CH_2COONa)_2.2H_2O$, 98%), urea ($NH_2CONH_2$, 98%) and sodium hydroxide (NaOH, 97%) are purchased from Sigma Aldrich and used as received. Potassium permanganate ($KMnO_4$, 98.5%), ethanol (CH_3CH_2OH, 98%) and silver nitrate ($AgNO_3$, 99 %) are purchased from Merck. Sulfuric acid (H_2SO_4, 90%) is purchased from Fischer Scientific. Ultrapure water of resistivity 18.2 MΩ cm, is acquired from a Millipore direct Q3UV system.

Cell assembly

A schematic representation of the cell assembly is shown in Fig. 1. Two **L** shaped Whatman filter paper strips are placed placed parallel to each other on a micro-slide glass plate such that the spacing between the long edges of the strip is 0.2 cm. One of the tail ends of each strip is immersed in the reservoirs containing anolyte (SPC + NaOH) and catholyte ($KMnO_4$ + H_2SO_4). Graphite sheets having dimensions 1.5 cm × 0.8 cm × 0.2 cm are used as electrodes and the active area of the electrodes that comes in contact with the paper strip is ~0.56 cm^2. A gel membrane is placed between the two strips adjacent to the electrodes, which allows the transport of ions and limits the mixing of anolyte and catholyte. Two absorbing pads made of tissue paper are placed at the other ends of strips to absorb the excess anolyte and catholyte. The absorbing pad acted as a sink for the anolyte and catholyte streams, and maintains their flow through the paper strip.

Preparation of gel electrolyte

The gel electrolyte is prepared by following a method described elsewhere [24]. Briefly, a solution of 1 g of acrylamide in 5 mL of ultra pure water is stirred and heated at 90 ^oC at 600 rpm for 10 min. A solution of 3 mg of ammonium persulfate, dissolved in 1 mL of ultra pure water is introduced into the acrylamide solution, accompanied by vigorous stirring, and heating for 10 more min. to form the gel. To this gel, 2 mL of 2 M H_2SO_4 in ultra pure water is added and stirred again at 600 rpm for 5 min. without heating. Electrolyte gels with other acid concentrations are prepared by following the same procedure, except for replacing the concentration of the acid by other concentrations (1, 3, 4, 5 M H_2SO_4).

Preparation of nanoparticles of Au, NiO and Au/NiO

Graphite sheets having dimensions of 1.5 cm × 0.8 cm × 0.2 cm are used as the electrodes. The graphite sheet also acted as a current collector for the system. To enhance the cell performance, the graphite electrodes are impregnated with Au, NiO and Au/NiO catalysts. For the preparation of Au nanoparticles, a method described elsewhere is followed. 0.5 wt% aqueous stock solution of $HAuCl_4{\cdot}3H_2O$ is prepared and stored in a refrigerator at 4 ^oC before use. 1 mL of $HAuCl_4$ solution and 42.5 µl of $AgNO_3$ (0.1 wt%) solution are mixed in a 10 mL beaker. Following this, 1 mL of an aqueous sodium citrate solution (1 wt%) is added into the beaker. Ultra pure water is further added such that the total volume of the resulting solution is 2.5 mL. The solution is kept in a refrigerator at 4 ^oC for 5 min. 47.5 mL of water is taken in a double necked round bottom flask fitted with a condenser and boiled under reflux conditions for 10 min. The cold mixture of $HAuCl_4{\cdot}3H_2O/AgNO_3$/citrate is introduced into the hot boiling water under vigorous stirring. The color of the solution changed from yellow to grey. Refluxing is continued with the mixture for 1 h and a wine-red colored solution of Au nanoparticles (NPs) is obtained [25].

For the preparation of Au/NiO composites, a method reported by Pan et al. [26], is employed. A solution with total 5 mmol of $HAuCl_4{\cdot}3H_2O$ and $Ni(NO_3)_2{\cdot}6H_2O$ is prepared in a mixed solvent containing 15 mL deionized water and 60 mL of ethanol, under agitation. The solution contained 0.2 mmol of $HAuCl_4{\cdot}3H_2O$ and 4.8 mmol of $Ni(NO_3)_2{\cdot}6H_2O$. To this solution, 0.3 g of dioctyl sulfosuccinate sodium salt (AOT, surfactant) and 20 mmol of urea are added and the mixture is stirred for 20 min. at room temperature. Finally, the mixture is transferred into a Teflon-lined stainless

steel autoclave, sealed and placed in an oven for 12 h at 120 °C. The resulting product is centrifuged, collected and washed first with ultrapure water, and then with absolute ethanol three times. The product is dried in a vacuum oven for 10 h maintained at 80 °C. The dry product is calcined at 350 °C for 3 h. The Au/NiO product is black in color. The product obtained is referred to as Au/NiO (with 11 wt% Au), by considering the weight of Au incorporated in the composite with respect to the weight of NiO formed, and by assuming complete conversions of Au^{3+} to Au^0, and the Ni-salt to NiO. Two more Au/NiO composites are prepared by varying the concentrations of $HAuCl_4 \cdot 3H_2O$ and $Ni(NO_3)_2 \cdot 6H_2O$, in the first step to (i) 0.1 and 4.9 mmol, and to (ii) 0.3 and 4.7 mmol. By repeating the same steps as mentioned above, the final products obtained are labelled as Au/NiO (with 5.11 wt% Au) and Au/NiO (with 16.8 wt% Au) respectively. Pristine NiO is also prepared using the same sequence of the above mentioned steps, except introducing Au precursor in the first step [26].

Characterization

An Autolab PSTAT 302N with a frequency response analyzer has been used for all electrochemical measurements (polarization curves, chronoamperometric and chronopotentiometric and impedance analysis). X-ray diffraction (XRD) patterns have been recorded for the catalysts on a PANalytical XPert XRD system with CuK_α radiation (λ = 1.5405 Å), and by using an operating voltage and current of 30 kV and 40 mA respectively. The absorption spectra of catalysts have been measured in the form of colloids using a UV-Visible spectrometer (P4 instruments) X-ray fluorescence (XRF) studies have been performed on the fuel and oxidant strips using a PANalytical X-ray fluorescence epsilon 3XL energy dispersive spectrometer, which provided elemental information on the strips. A Zeiss scanning electron microscope (SEM) is used for recording the SEM images of samples. Transmission electron microscope (Philips TEM CM 200) with a resolution of 2.4 Å, is used for characterizing the catalysts by first dispersing the samples in isopropanol, and then extracting a thin layer onto carbon coated copper grids. The sample coated grids are used after solvent evaporation at room temperature.

5 Keywords

Fuel cell, Sodium percarbonate, Nanoparticles, Power density, Micro-nano devices.

6 TOC

Text for TOC- **Power of Paper**: Porous paper supported low cost mixed media fuel cell delivers sufficient power density (2.66 mW/cm^2) for powering micro-nano devices.

Figure for TOC

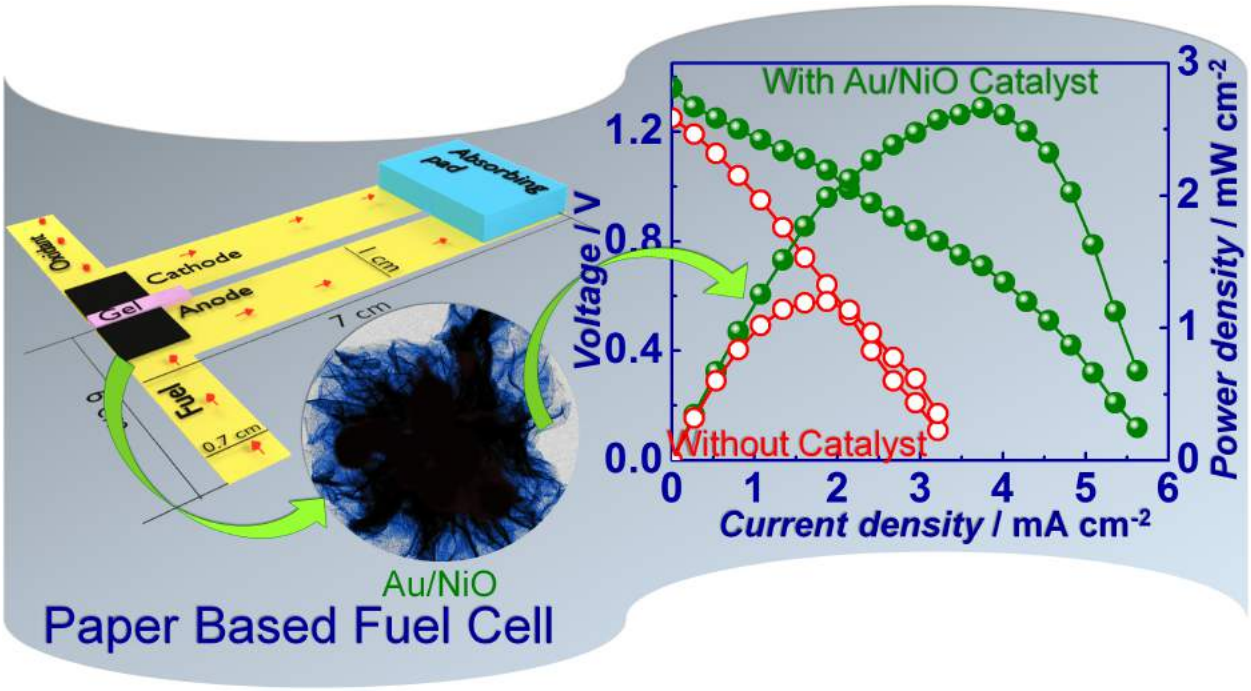

References

[1] S. A. M. Shaegh,, N-T. Nguyen, S. H. Chan, *Int. J. Hydrog. Energy*, **2011**, *36*, 5675-5694.

[2] H. B. Park, K. H. Lee, H. J. Sung, *J. Power Sources*, **2013**, *226*, 266-271.

[3] K. S. Salloum, J. R. Hayes, C. A. Friesen, J. D. Posner, *J. Power Sources*, **2008**, *180*, 243-252.

[4] M. Gowdhamamoorthi, A. Arun, S. Kiruthika, B. Muthukumaran, *J. Mater.*, **2013**, *2013*, 548026.

[5] E. R. Chiban, L. J. Markoski, A. Wieckowski, P. J. Kenis, *J. Power Sources*, **2004**, *128*, 54-60.

[6] S. A. M. Shaegh, N-T. Nguyen, S. H. Chan, W. Zhou, *Int. J. Hydrog. Energy*, **2012**, *37*, 3466-3476.

[7] E. Kjeang, A. G. Brolo, D. A. Harrington, N. Djilali, D. Sinton, *J. Electrochem. Soc.*, **2007**, *154*, B1220–B1226.

[8] J. P. Esquivel, F. J. Del Campo, J. L. Gomez de la Fuente, S. Rojas, N. Sabate, *Energy Environ. Sci.*, **2014**, *7*, 1744-1749.

[9] S. Lal, V. M. Janardhanan, M. Deepa, A. Sagar, K. C. Sahu, *J. Electrochem. Soc.*, **2015**, *162*, F1402-F1407.

[10] A. Fraiwan, S. Mukherjee, S. Sundermier, H. S. Lee, S. Choi, *Biosens. Bioelectron*, **2013**, *49*, 410-414.

[11] X. Yan, F. Meng, Y. Xie, J. Liu, Y. Ding, *Sci. Rep.*, **2012**, *2*, 1-7.

[12] M. Yadav, Q. Xu, *Energy Environ. Sci.*, **2012**, *5*, 9698-9725.

[13] C. Forrestal, Z. Huang, Z. J. Ren, *Bioresource Technol.*, **2014**, *172*, 429-432.

[14] A. McKillop, W. R. Sanderson, *Tetrahedron*, **1995**, *51*, 6145-6166.

[15] R. K. Arun, S.Halder, N.Chanda, S.Chakraborty, *Lab. Chip*, **2014**, *14(10)*, 1661.

[16] M. H. Sun, G. V. Casquillas, S. S. Guo, J. Shi, H. Ji, Q. Ouyang, Y. Chen, *Microelectron. Eng.*, **2007**, *84*, 1182-1185.

[17] J. P. Esquivel, F. J. Del Campo, J. L. G. De La Fuente, S. Rojas, N. Sabate, *17th International Conference on Miniaturized Systems for Chemistry and Life Sciences, MicroTAS*, **2013**, *2*, 1251-1253

[18] F. Pei, Y. Wang, X. Wang, P. Y. He, L. Liu, Y. Xu, H. Wang, *Fuel Cells*, **2011**, *5*11, 595-602.

[19] T. Yang, L. Zhang, X. Li, D. Xia, *J. Alloys Compd.*, **2010**, *492*, 83–87.

[20] T. Yang, C. M. R. de Almeida, D. Ramasamy, F. J. A. Loureiro, *J. Power Sources*, **2014**, *269*, 46–53.

[21] T. Yang, D. Ramasamy, R. P. Queiros, F. J. A. Loureiro, C. M. R. de Almeida, P. S. Julia, *Int. J. Hydrogen Energy*, **2015**, *40*, 4980–4988.

[22] M. A. Smith, *IEEE Transactions on Industry Applications*, **1982**, *4(IA-18)*, 431-434.

[23] E. Kjeang, J. McKechnie, D. Sinton, N. Djilali, *J. Power Sources*, **2007**, *168*, 379-390.

[24] Q. Tang, G. Qian, K. Huang, *RSC Advances*, **2012**, *2*, 10238-10244.

[25] H. Xia, S. Bai, J. Hartmann, D. Wang. *Langmuir*, **2009**, *26*, 3585-3589.

[26] L. Pan, L. Shen, L. Li, Q. Zhu, *J. Mater. Sci.: Mater. Electron.*, **2009**, *27*, 3065-3070.

[27] B. Prasad, V. M. Janardhanan, *J. Electrochem. Soc.*, **2014**, *161*, 208-213.

[28] V. M. Janardhanan, D. S. Monder, *J. Electrochem. Soc.* , **2014**, *161*, F1427-F1436.

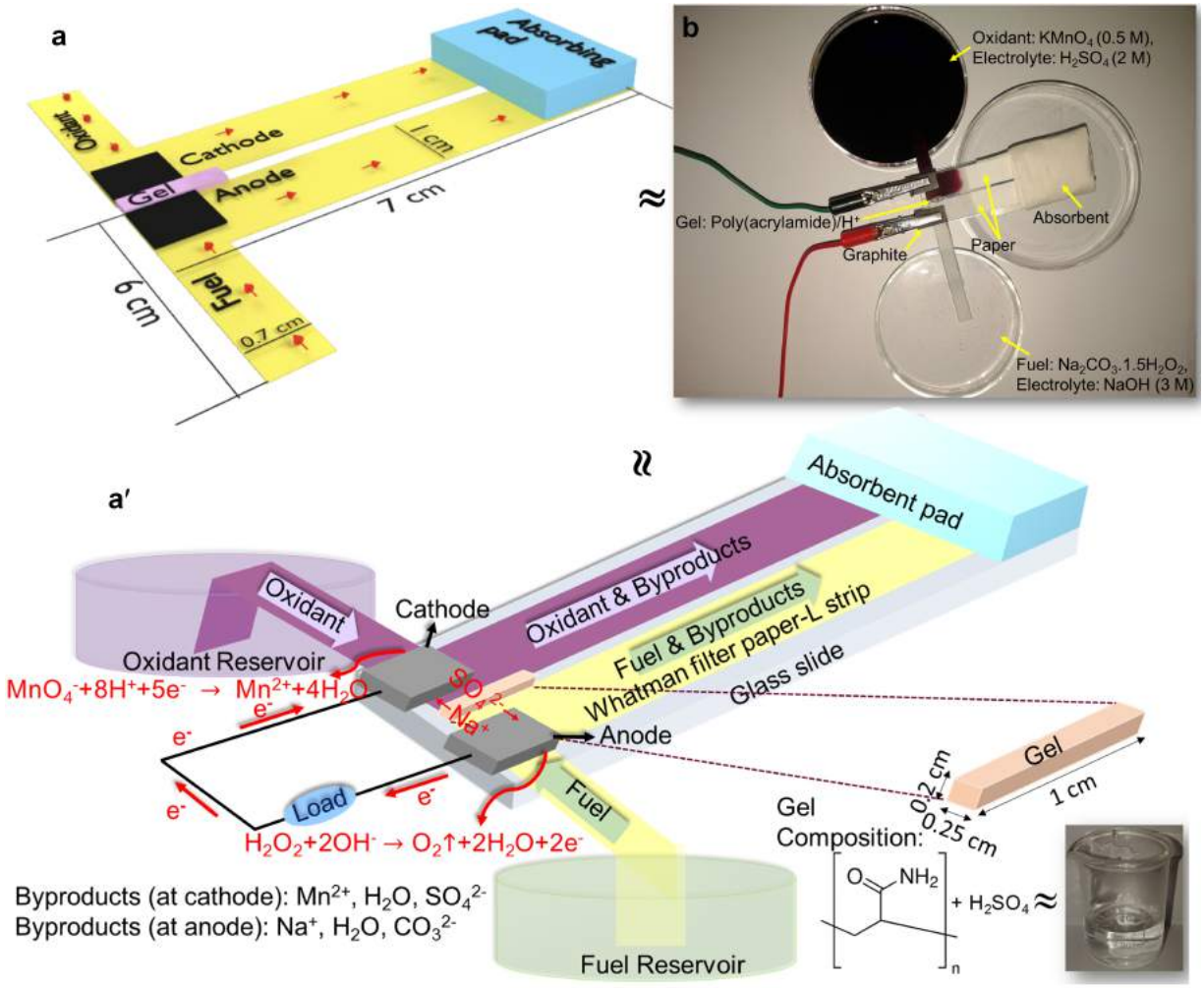

Figure 1: (a) Schematic of a T-shaped mixed media paper based fuel cell, (a) cartoon of the cell showing the redox reactions, electron and ion movement and (b) a photograph of a working T-shaped fuel cell.

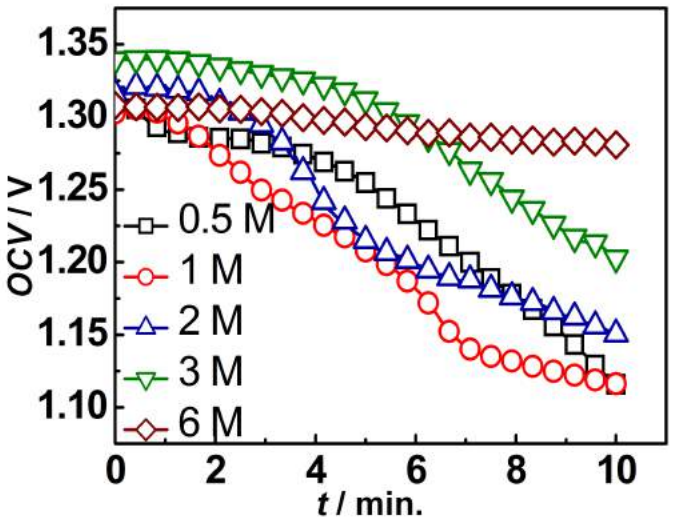

Figure 2: Variation of OCV for different concentrations of SPC. For all cases, 3 M NaOH is used along with SPC as the anolyte and 0.5 M $KMnO_4$ with 2 M H_2SO_4 is used as the catholyte.

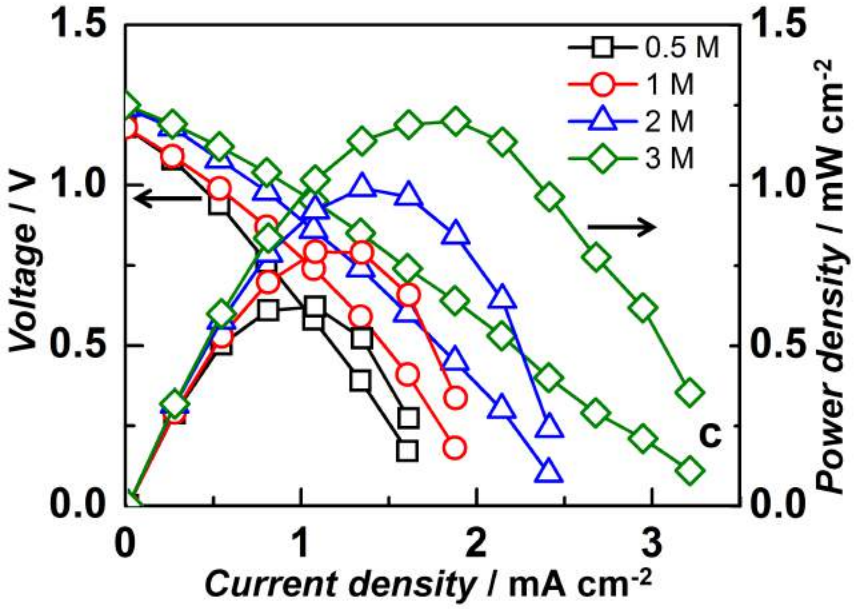

Figure 3: Cell performance for different concentrations of SPC. For all cases 3 M NaOH is used along with SPC as the anolyte and 0.5 M $KMnO_4$ with 2 M H_2SO_4 is used as the catholyte.

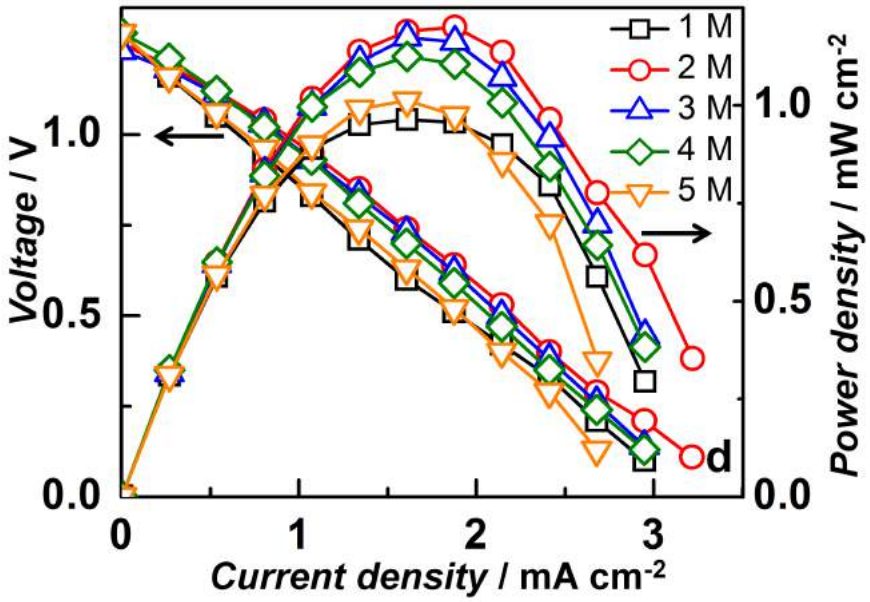

Figure 4: Cell performance for different concentrations of H_2SO_4 in the gel. Anolyte is 3 M SPC with 3 M NaOH and catholyte is 0.5 M $KMnO_4$ with 2 M H_2SO_4.

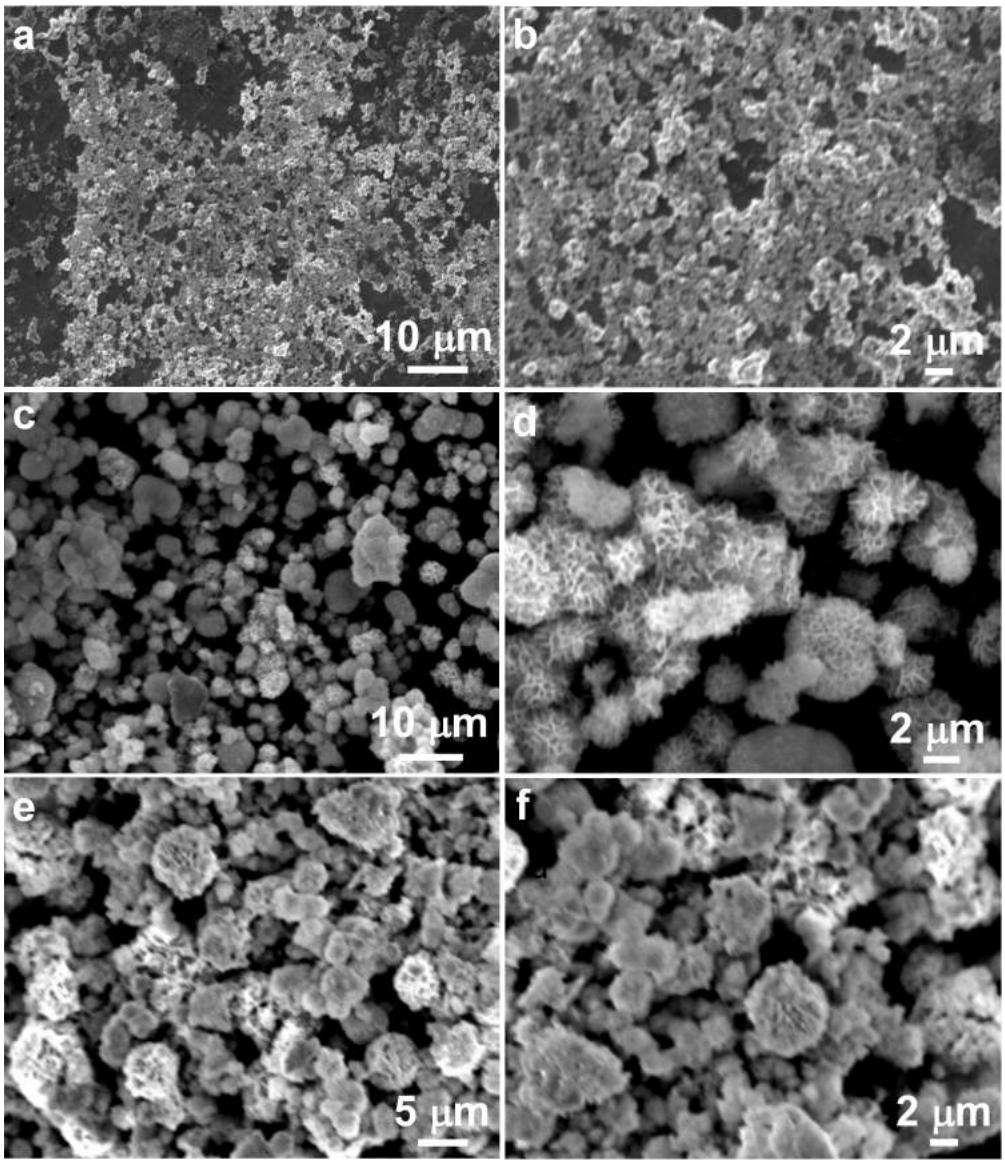

Figure 5: SEM images of different catalysts: (a, b) Au NPs, (c,d) NiO and (e, f) Au/NiO composite (with 11 wt% Au), at different magnifications.

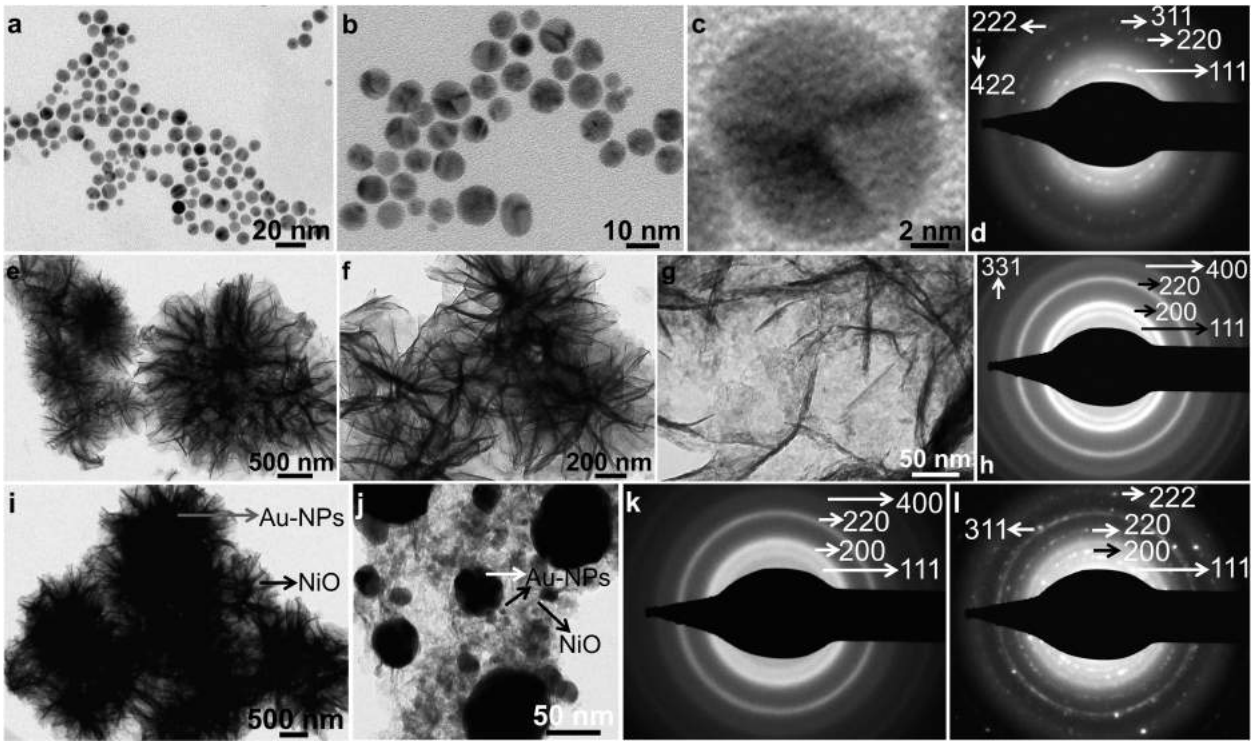

Figure 6: TEM images of (a-c) Au NPs at different magnifications, (d) SAED pattern of Au NPs, (e-g) TEM images of pristine NiO at different magnifications, (h) SAED pattern of pristine NiO, (i,j) TEM images- and (k,l) SAED patterns- of the Au/NiO (with 11 wt% Au) composite.

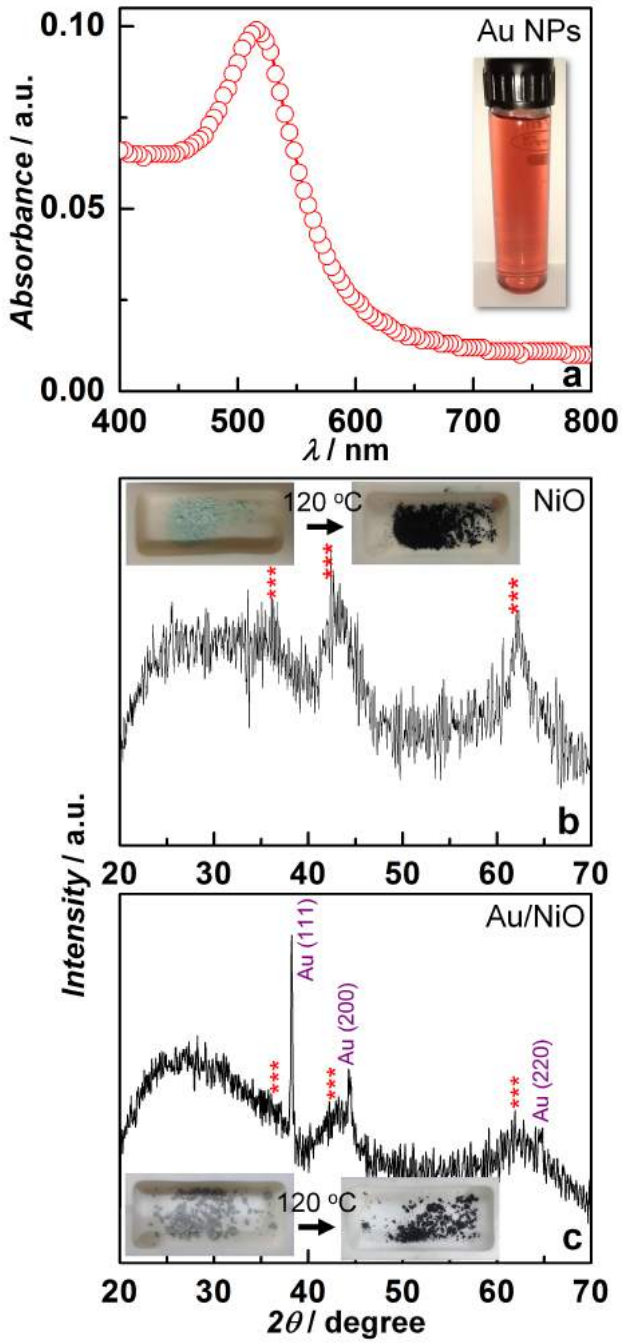

Figure 7: (a) UV-Visible spectra of Au NPs and inset is a photograph of the colloid, XRD patterns of (c) NiO and (d) Au/NiO (with 11 wt% Au) composite, and their photographs are shown as insets.

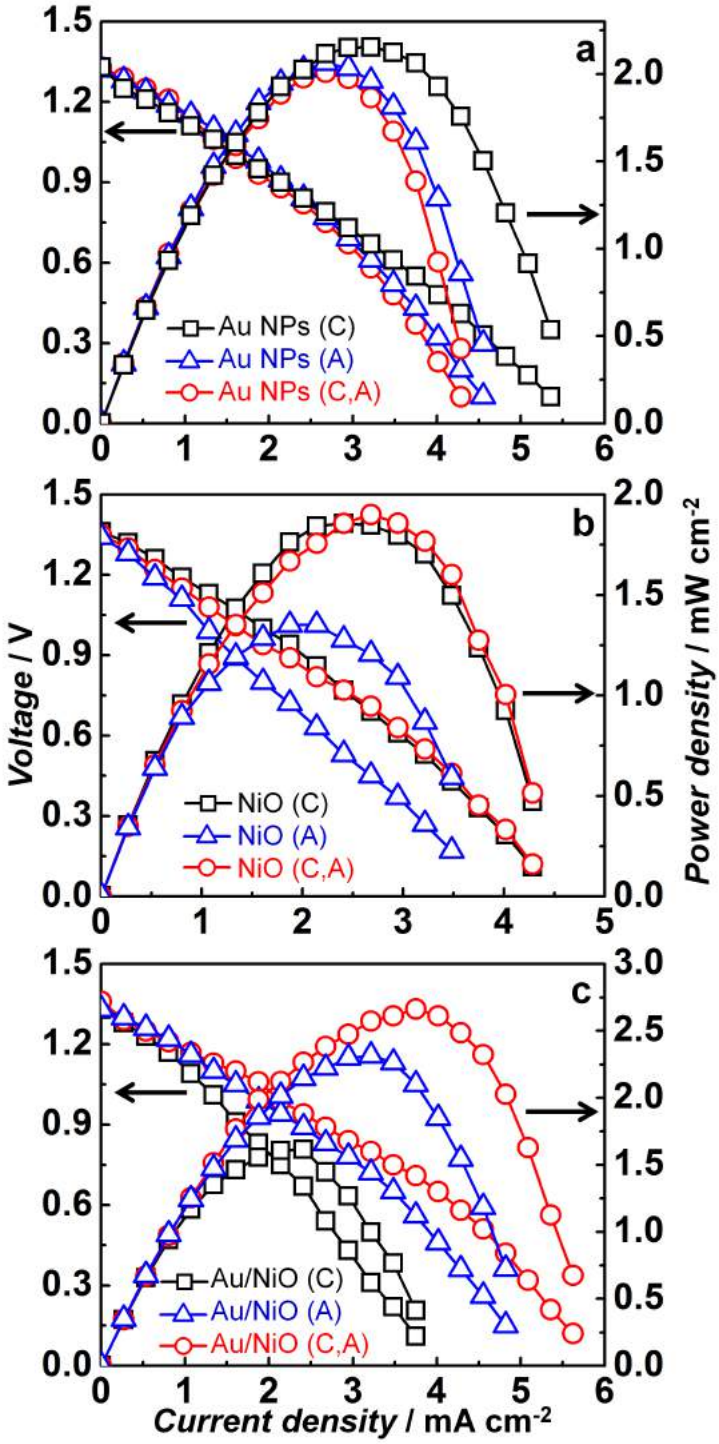

Figure 8: Cell performance with various catalyst loading at the anode and cathode. Anolyte: 3 M SPC with 3 M NaOH. Catholyte: 0.5 M $KMnO_4$ with 2 M H_2SO_4.

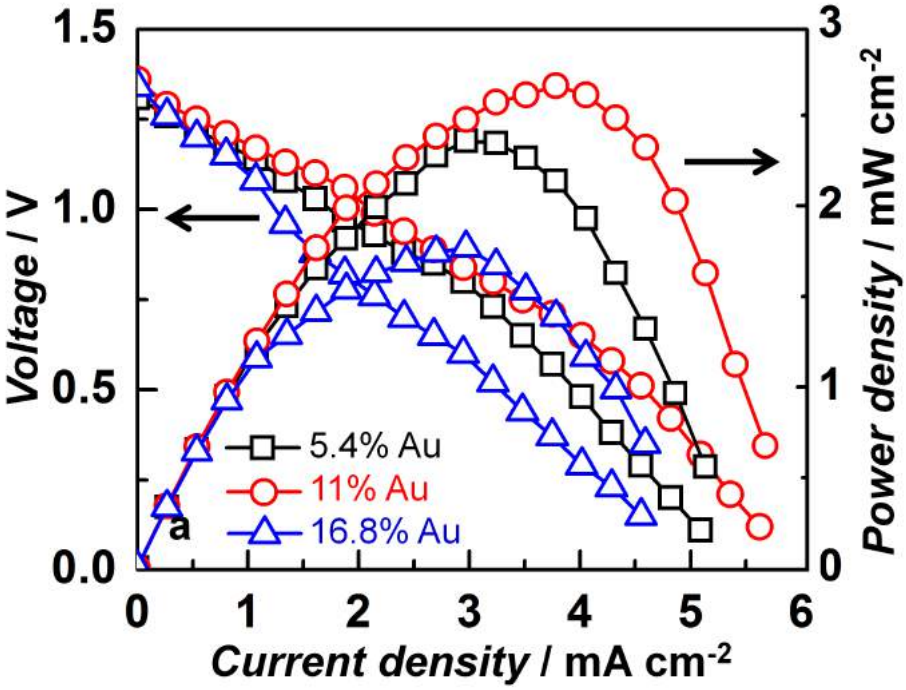

Figure 9: Polarization curves for T-shaped mixed media paper based fuel cells with Au/NiO composites (having different proportions of Au content: 2,4 % and 6%) deposited as catalysts on both electrodes: (a) voltage versus current density and (b) power density versus current density curves. In (a and b), all cells were operated under optimum conditions: with 3 M SPC dissolved in 3 M NaOH as the fuel, 0.5 M $KMnO_4$ (in 2 M H_2SO_4) as the oxidant and a 2 M H^+ conducting gel as the electrolyte.

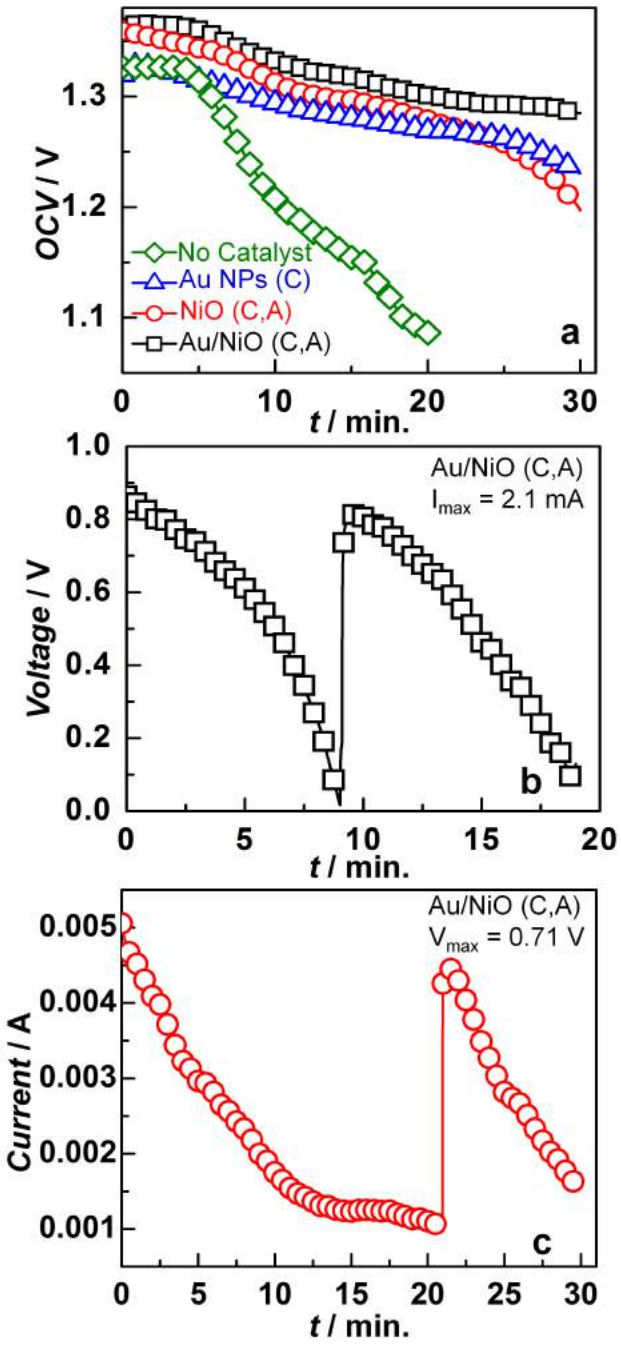

Figure 10: (a) Comparison of OCV versus time curves for T-shaped mixed media cells with and without catalysts. (b) Voltage versus time curve under a constant current of 2.1 m*A* and (c) current versus time curve at a constant voltage of 0.71 *V* , with Au/NiO (with 11 wt% Au) deposited on cathode and anode, in (b and c). In (a-c), all cells are operated under optimum conditions: with 3 M SPC dissolved in 3 M NaOH as the fuel, 0.5 M $KMnO_4$ (in 2 M H_2SO_4) as the oxidant and a 2 M H^+ conducting gel as the electrolyte. C and A: imply cathode and anode respectively

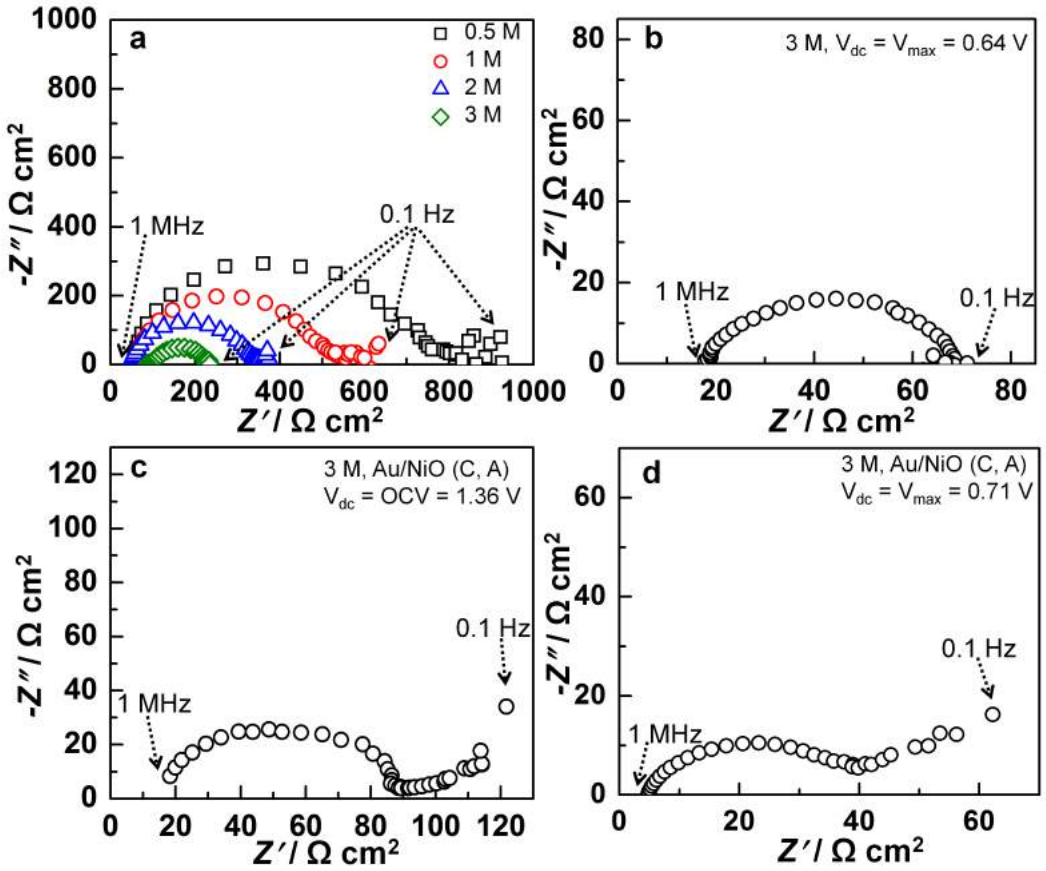

Figure 11: Nyquist plots for T-shaped mixed media cells (a) with varying concentration of SPC fuel from 0.5 M to 3 M at their respective OCVs (with no catalyst) and with 3 M SPC fuel concentration in (b-d): (b) at a set potential of 0.64 *V* (with no catalyst), (c) with Au/NiO (with 11 wt% Au) as catalyst on both electrodes at OCV and (d) with Au/NiO (with 11 wt% Au) as catalyst on both electrodes at 0.71 *V*. In (a-d), all cells are operated with 0.5 M $KMnO_4$ (in 2 M H_2SO_4) as the oxidant and a 2 M H^+ conducting gel as the electrolyte.